A Fluoride-Driven Ionic Gate Based on a 4-Aminophenylboronic Acid-Functionalized Asymmetric Single Nanochannel

Qian Liu,[†,⊥] Kai Xiao,[‡,⊥] Liping Wen,[*,‡] Yang Dong,[†] Ganhua Xie,[‡] Zhen Zhang,[‡] Zhishan Bo,[*,†] and Lei Jiang[*,‡]

[†]Beijing Key Laboratory of Energy Conversion and Storage Materials, College of Chemistry, Key Laboratory of Theoretical and Computational Photochemistry, Ministry of Education, Beijing Normal University, Beijing 100875, P. R. China and [‡]Beijing National Laboratory for Molecular Sciences (BNLMS), Key Laboratory of Organic Solids, Institute of Chemistry, Chinese Academy of Sciences, Beijing 100190, P. R. China. [⊥]Q.L. and K.X. contributed equally to the study.

ABSTRACT Fluorine is one of the human body's required trace elements. Imbalanced fluoride levels severely affect the normal functioning of living organisms. In this article, an anion-regulated synthetic nanochannel is described. A fluoride-driven ionic gate was developed by immobilizing a fluoride-responsive functional molecule, 4-aminophenylboronic acid, onto a single conical polyimide nanochannel. When the ionic gate was in the presence of fluoride, the boron bound F^-, and the hybridization of the boron center changed from sp^2 to sp^3. Thus, negatively charged monofluoride adduct ($RB(OH)_2F^-$), difluoride adduct ($RB(OH)F_2^-$), and trifluoride adduct (RBF_3^-) modified surfaces with different wettability would be formed successively by increasing the concentration of F^-. On the basis of the variation of surface charge and wettability, the nanochannel can actualize reversible switching between the "off" state and the "on" state in the absence and presence of F^-, respectively. As an anion-regulated synthetic nanochannel, this fluoride-driven ionic gate was characterized by measuring ionic current, which possesses high sensitivity, fine selectivity, and strong stability. Thus, this gate may show great promise for use in biosensors, water quality monitoring, and drug delivery.

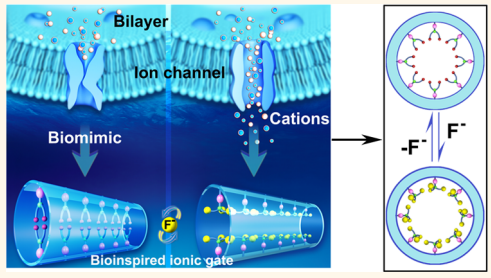

KEYWORDS: fluoride-driven · gate · 4-aminophenylboronic acid · nanochannel

Living organisms harbor many classes of significant particles, including cations, anions, and neutral molecules.[1] Cations, which often influence normal bodily function, are a case in point. For example, Na^+ and K^+ underlie electrical signaling in the nervous system;[2] Zn^{2+} and Ca^{2+} regulate physiological function in the human body;[3,4] Al^{3+} affects the human nervous system and induces many diseases.[5] Similar to cations, anions also exist widely in living organisms and play an essential role in biological processes. Anions are suspected to participate in 70% of all enzymatic reactions.[6−9] Halogen ions are the most common anions in biological systems. They have garnered greater attention because of their unique biological, chemical, and physical properties.[10,11] Among the halogens, fluorine is a required trace element in the human body.[12,13] A lack of fluoride can cause dental caries and osteoporosis.[14,15] More seriously, a fluoride deficit can affect human growth and development. Meanwhile, the acute intake of a large dose or chronic ingestion of lower doses of fluoride can result in acute gastric and kidney disorders, dental and skeletal fluorosis, immune system disruption, and even death.[16] At the same time, the uptake and metabolism of F^- seriously affects the growth of plants and animals.[17] Given the enormous increase of industrially produced aluminum fluoride discharged into the environment, there are greater threats to living systems.[18] Therefore, it is important to explore new approaches to fluorine regulation in living organisms.

In living organisms, cells have a variety of ion channels to regulate many critical cellular functions by continuously exchanging ions with the exterior environment to balance electrolytes.[19,20] To adequately understand ionic transport in channels, carbon nanotubes,[21−23] supramolecular channels,[24,25]

* Address correspondence to wlp@iccas.ac.cn, zsbo@bnu.edu.cn, jianglei@iccas.ac.cn.

Received for review August 13, 2014 and accepted December 7, 2014.

Published online December 07, 2014
10.1021/nn506257c

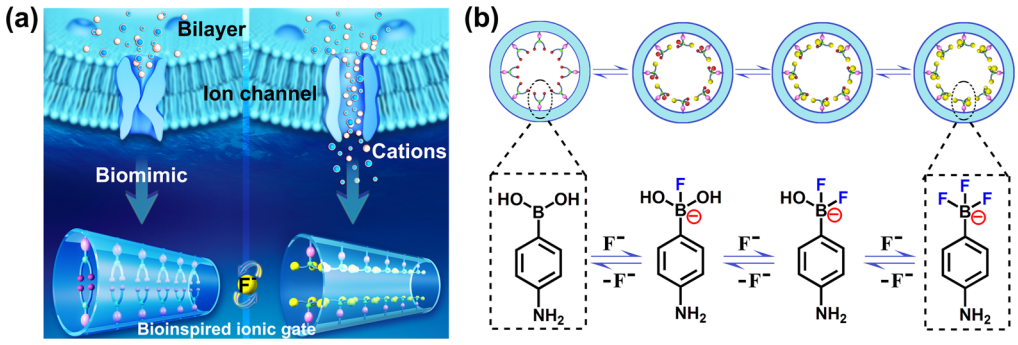

Scheme 1. Schematic demonstration of the simplified fluoride-driven ionic gate: (a) an artificial fluoride-driven ionic single nanochannel; (b) schematic representation of the reversible switching between BA, $RB(OH)_2F^-$, $RB(OH)F_2^-$, and RBF_3^-.

and solid-state synthetic nanochannels,[26] *etc.* have been applied to bionics. Among them, solid-state synthetic nanochannels have developed rapidly in recent years. Nanochannels are flexible in terms of geometry and size, stable under a variety of conditions, and addressable with various functionalities on the surface.[27] Many kinds of solid-state synthetic nanochannels regulated by environmental stimuli have been realized, such as pH,[28−31] temperature,[32,33] ligands,[34−36] light,[37−39] and even electric fields.[40,41] To further expand the application of solid-state synthetic nanochannels in the field of ionic regulation, many functional groups that are responsive to specific ions or molecules have been introduced into solid-state synthetic nanochannels.[42,43] The presence of specific ions or molecules causes the functional groups to change drastically. Primarily, the diameter, surface charge, and wettability vary.[44−48] Transformations caused by a change in surface charge and wettability are faster and more obvious. Given the importance of regulating cations (*e.g.,* K^+,[49] Hg^{2+},[50] Zn^{2+},[4] Ca^{2+}[51], and Fe^{3+},[52] *etc.*), it is unsurprising that cationic gates based on solid-state synthetic nanochannels have been widely investigated. However, to date, no solid-state synthetic nanochannels have been modified with anion-responsive functional molecules. More importantly, ionic gates that are responsive to halogen ions have not been implemented yet. Accordingly, a fluoride-regulated nanochannel will find application in bionics, biosensors, controlled nanofluids, and drug delivery systems. Hence, building a fluoride-driven ionic gate *in vitro* is important.

In this article, we report a novel fluoride-driven ionic gate obtained by immobilizing a fluoride-responsive molecule onto a single conical polyimide (PI) nanochannel. Recently, many F^--responsive molecules and functional groups have been reported. These molecules and functional groups include amides,[53,54] urea,[55] boronic acid,[56−58] vitamin B_6,[59] indole,[12] and calixpyrrole[60] among others. Out of these molecules, phenylboronic acid attracts our attention because of its unique chemical properties.[17] For example, phenylboronic acid has good solubility in water, superior selectivity, high sensitivity, and fine reversibility. When boron binds F^-, the hybridization of the boron center changes from sp^2 to sp^3 and negatively charged boron−fluorine complexes forms. Thus, the surface charge transforms from neutral to negative.[17,61] The wettability also changes upon fluoride binding. On the basis of the wettability and surface charge variation, we modified 4-aminophenylboronic acid (APBA) in the single conical polyimide nanochannel to obtain the first fluoride-driven ionic gate. This system is advantageous because visualization is simple, it is devoid of contamination from aqueous solvents, and it can possibly be applied to bionic and living systems.

As shown in Scheme 1a, the mechanism of this fluoride-driven ionic gate is similar to the voltage-gated ion channels in cell membranes. When ions are transported through the channel, the channel is in the "on" state. Otherwise, the channel is in the "off" state. This on/off property can be demonstrated in the fluoride-driven gate by measuring the ionic current through functionalized nanochannels. For a conical nanochannel with permanent surface charge, the asymmetric shape allows the system to exhibit ionic current rectification, which can preferentially transport cations/anions from the small opening (tip) to the large opening (base) of the channel. Rectification emerges owing to the intrinsic asymmetry of the electrochemical potential of the channel.[62] The values can be visualized by measuring current−voltage (I−V) curves under symmetrical electrolyte conditions. As shown in Scheme 1b, the APBA immobilized on the nanochannel can form negatively charged tetrahedral fluoride adducts, including monofluoride adducts ($RB(OH)_2F^-$), difluoride adducts ($RB(OH)F_2^-$), and trifluoride adducts (RBF_3^-) upon addition or removal of F^-.[17] Thus, we obtained a fluoride-driven ionic gate with high sensitivity and selectivity. This gate can potentially be employed in bionic systems.

RESULTS AND DISCUSSION

The specific F^- responsiveness of APBA was measured by UV−vis absorption (Figure 1a), fluorescence spectroscopy (Figure 1b), and ^{19}F NMR spectra

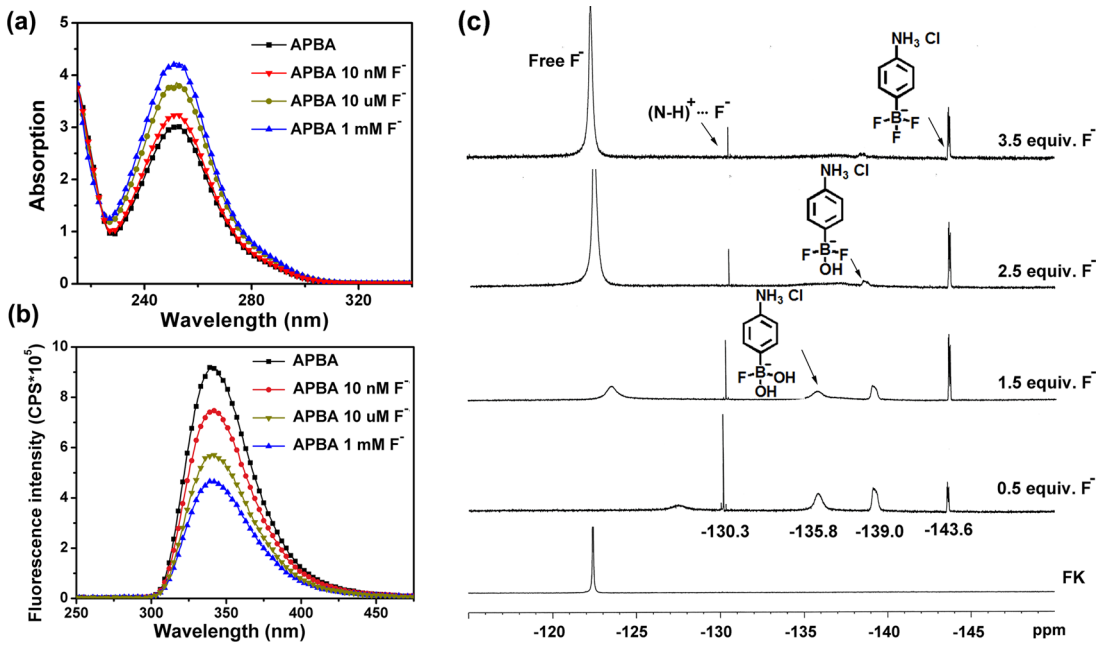

Figure 1. Changes in UV−vis absorption spectra (a) and fluorescence emission spectra (b) of APBA (0.8 mM) at 25 °C in water upon the addition of 10 nM, 10 μM, and 1 mM KF. (c) ^{19}F NMR spectra of 6.24 mg of APBA with different equiv F^- (0.5, 1.5, 2.5, and 3.5) in 0.5 mL of D_2O.

(Figure 1c). As shown in Figure 1a, APBA (0.8 mM) in water with a different concentration of F^- exhibited one broad absorption band ranging from 230 to 300 nm with a maximum located at 251 nm. However, the UV−vis absorption intensity of APBA was enhanced gradually with increasing F^- concentrations. Meanwhile, the fluorescence of APBA was dramatically altered when F^- was added. The emission band of APBA at 340 nm progressively decreased with F^- added due to the formation of tetrahedral fluoride adducts between APBA and fluoride. The tetrahedral fluoride adduct can quench the fluorescence of APBA by a photoinduced electron transfer (PET) mechanism.[17] ^{19}F NMR spectra of APBA with different equiv F^- (0.5, 1.5, 2.5, and 3.5) in D_2O was also obtained. As shown in Figure 1c, the peak at −122.4 ppm was free F^- in D_2O, and new peaks appeared upon the addition of 0.5, 1.5, 2.5, and 3.5 equiv F^- to 72 mM APBA. On the basis of the references,[63−66] it is easy to explain the ^{19}F NMR spectra. The peak at −130.3 ppm corresponds to $(N-H)^+\cdots F^-$, and the other three peaks at −135.8, −139.0, and −143.6 ppm correspond to $RB(OH)_2F^-$, $RB(OH)F_2^-$, and RBF_3^-, respectively. Meanwhile, $RB(OH)_2F^-$, $RB(OH)F_2^-$, and RBF_3^- existed in the system when 0.5 equiv F^- was added to 1.0 equiv APBA. The peaks of $RB(OH)_2F^-$ and $RB(OH)F_2^-$ decreased, while the peak of RBF_3^- increased with the addition of 1.5 equiv F^-. When the content of F^- increased to 2.5 equiv F^-, the peak of $RB(OH)_2F^-$ almost disappeared and the peak of $RB(OH)F_2^-$ decreased obviously, indicating that most $RB(OH)_2F^-$ was converted to RBF_3^- with a small amount of $RB(OH)F_2^-$ and a lot of RBF_3^- existing in the system. With more F^- (3.5 equiv F^-), the peak of $RB(OH)F_2^-$ disappeared gradually, indicating that only RBF_3^- existed under the condition of abundant F^-. The species detected by ^{19}F NMR are consistent with the fluoride adducts depicted in Scheme 1b and the observed spectroscopy behavior which indicates that APBA can respond to F^-.

Current−voltage ($I-V$) characteristics of the single PI nanochannel before and after modification with APBA and in the absence or presence of F^- have been examined with current measurements. As shown in Figure 2a, the nonmodified single PI nanochannel presented a fine rectified $I-V$ curve in 0.1 M $NaNO_3$ at pH 6.77 owing to its negative charge and conical shape. Notably, no change was found when 100 nM F^- was added to the nonmodified single PI nanochannel. With the APBA immobilized on the nanochannel, the current decreased markedly, which could be explained by a change in surface charge, effective pore size, and wettability. The difference between these two $I-V$ curves (the dark yellow square and purple triangle) indicates the success of APBA immobilization. XPS tests on the APBA-modified PI surface further confirm the binding process (Supporting Information, Figure S2, Table S1, and Table S2). When 100 nM F^- was added to activate the APBA-modified single nanochannel, the current doubled from −5 nA (purple triangle) to −10 nA (navy inverted triangle). The switch can be explained by the binding of F^- to B, which changes the configuration of boron from planar to tetrahedral, thereby altering the wettability and generating a negative charge. This phenomenon can also be reflected by the current ratio I_{F^-}/I (the ionic current after/before interacting with F^- at −2.0 V), which are shown in

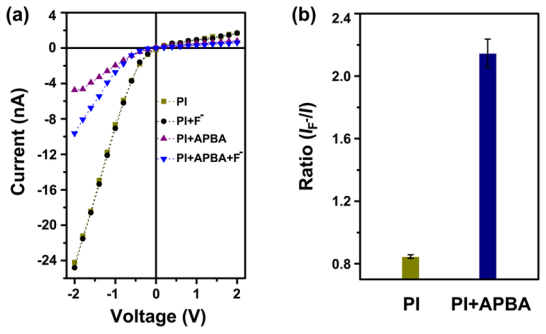

Figure 2. Asymmetric ionic transport properties: (a) current−voltage characteristics of a conical nanochannel in 0.1 M $NaNO_3$ (pH 6.77), prior to (dark yellow square and black circle) and after (purple triangle and navy inverted triangle) modification with 10 mM APBA in the absence (dark yellow square and purple triangle) and presence (black circle and navy inverted triangle) of 100 nM F^-; (b) current ratios of nonmodified (dark yellow column) and APBA-modified (navy column) nanochannel which were calculated by the ionic current measured in the presence of F^- *versus* the absence of F^- at −2.0 V.

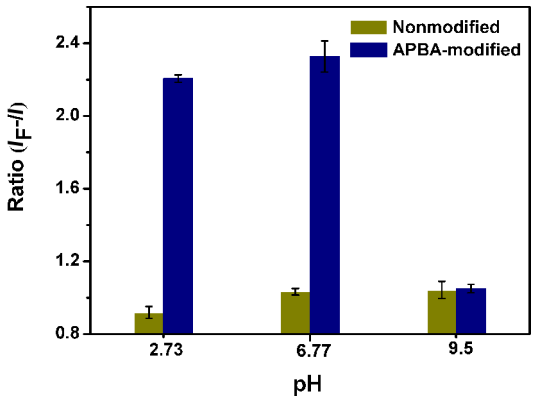

Figure 3. Current ratios of the nonmodified (dark yellow column) and APBA-modified (navy column) nanochannel at different pH values (2.73, 6.77, and 9.5) which were calculated by the ionic current measured in the presence of 100 nM F^- *versus* the absence of F^- at −2.0 V.

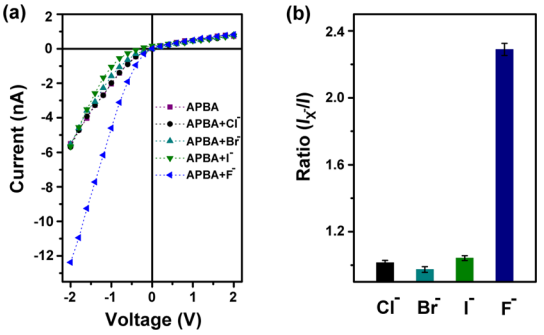

Figure 4. Selectivity of fluoride-driven ionic gate: (a) $I-V$ curves of the single nanochannel after APBA modification in 0.1 M $NaNO_3$ (pH 6.77) without (purple square) or with the addition of 100 nM Cl^- (black circle), Br^- (cyan triangle), I^- (green inverted triangle), and F^- (navy left triangle), respectively. (b) The current ratios after modification with APBA in the presence of 100 nM Cl^- (black column), Br^- (cyan column), I^- (green column), and F^- (navy column).

Figure 2b. A dramatic difference between the nonmodified (approximately 0.8) and APBA-modified (approximately 2.2) nanochannel I_F^-/I ratios was observed. Therefore, it is concluded that F^- can regulate the APBA-modified nanochannel efficiently.

The current−voltage characteristics at different pH values (2.73, 6.77, and 9.5) in 0.1 M $NaNO_3$ are presented in Figure 3. Prior to modification with APBA, the current ratios (I_F^-/I) of the nonmodified nanochannel were approximately 1, irrespective of pH conditions, indicating that F^- has no influence on the nonmodified nanochannel. After modification with APBA, obvious pH-dependent differences on current ratios (I_F^-/I) with 100 nM F^- were shown. At pH 2.73 and pH 6.77, the current ratios (I_F^-/I) of APBA-modified nanochannels distinctly increased to ∼2.3, which suggests that the APBA-modified nanochannel can respond to F^- efficiently under acidic and neutral conditions. However, under alkaline conditions (pH 9.5), no distinct activated property was observed after the modification ($I-V$ curves were shown in Supporting Information, Figure S3). Notably, under alkaline conditions, hydroxyl ions can interact with the boron center (in a similar fashion to the fluorine anion), converting the tetrahedral fluoride adduct to $RB(OH)_3^-$.[57,67] Hence, an efficient response of the APBA-modified nanochannel to F^- could be realized under acidic and neutral conditions. Moreover, the reversibility of the fluoride-driven ionic gate can be implemented by adjusting the pH to alkaline values.

To confirm the selectivity of the fluoride-driven ionic gate, Cl^-, Br^-, and I^- were added to the APBA-modified nanochannel. The current at −2.0 V increased from −5.5 nA (the purple square) to −12.7 nA (the navy left triangle) after activation with 100 nM F^-. However, unlike the F^--activated phenomenon, the current of the nanochannel remained unchanged around −5.5 nA with the addition of 100 nM Cl^-, Br^-, and I^- (as shown in Figure 4a). Cl^-, Br^-, and I^- cannot bind to the boron atom effectively and, as a result, are unable to induce distinct surface charge variation in the APBA-modified nanochannel. Figure 4b shows the difference between the current ratios (I_X^-/I). Current ratios are calculated as the current in the presence of the halogen anion (F^-, Cl^-, Br^-, and I^-) divided by the current of the single conical nanochannel after modification with APBA at −2.0 V. The current ratios after interacting with Cl^-, Br^-, and I^- were 1.0 (the black column), 0.9 (the cyan column), and 1.0 (the green column), respectively. However, the current ratio after F^- binding increased to 2.3 (the navy column), which was much more dramatic than increases due to Cl^-, Br^-, and I^- addition. This result indicates that this fluoride-driven ionic gate is highly selective for F^-. This selective property can also be confirmed by fluorescence spectroscopy.[17,68]

The concentration of F^- has a strong impact on the fraction of the fluoride-driven ionic gate in the "on"

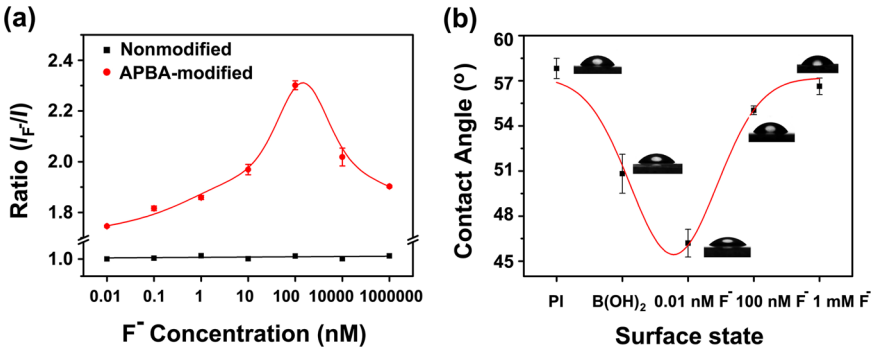

Figure 5. (a) Relationship between the current ratios and the concentration of F^- before (black) and after (red) modification with APBA to the inner surface of the single conical nanochannel. To the nonmodified, the current ratios remained unchanged near 1.0 with increasing F^- (red). After modification, current ratio increased gradually with increasing F^- from 0.01 to 100 nM. From 100 nM, current ratios decreased gradually again. (b) The variation of wettability for a flat PI film before (the first droplet) and after (the second droplet) modification with APBA, and then disposed by different concentrations of F^- (0.01 nM, 100 nM, and 1 mM).

state as expressed by the current ratios ($I_F{}^-/I$) of the APBA-modified nanochannel. As shown in Figure 5a, the current ratios of nonmodified nanochannel remain unchanged near 1.0 with an increase in F^- concentration. After modification with APBA, a remarkable change was observed with varying concentration of F^-. The current ratio first increased from 1.6 to 2.3 gradually as the concentration of F^- increased from 0.01 nM to 100 nM. After reaching the maximum value, the current ratio dropped and leveled off to approximately 1.9 as F^- concentrations continued to increase (from 100 nM to 1 mM). This unconventional phenomenon can be attributed to the synergy of surface charge and wettability. At the beginning, the influence of surface charge predominates. When the concentration of F^- is low (0.01 nM to 100 nM), most of the boronic acid immobilized on the nanochannel is in the form of a monofluoride adduct ($RB(OH)_2F^-$). The current ratio increases gradually due to the formation of a negative charge. Subsequently, the surface negative charges become saturated by the addition of F^- (100 nM to 1 mM). Thus, the impact of wettability predominates in the process of conversion from $RB(OH)_2F^-$ to RBF_3^- with the increasing of F^- concentration, and the current ratio is accordingly reduced. The current ratio will plateau at a level of 1.9 because that is where the surface charge and wettability remain unchanged with all of the boron atoms binding with F^- in the form of RBF_3^-.

This inference is also verified by contact angle measurements, which show the wettability variation of the APBA-modified PI surface under augmented F^- concentrations (as shown in Figure 5b). The mean water contact angle of the flat PI film which was prepared under the same conditions as the single nanochannel membrane was 58 ± 0.6°. After the PI film was modified with APBA, the mean water contact angle decreased to 51 ± 1.2°, resulting from the hydrophilicity of boronic acid. Once the APBA-modified PI film was activated by different concentrations of

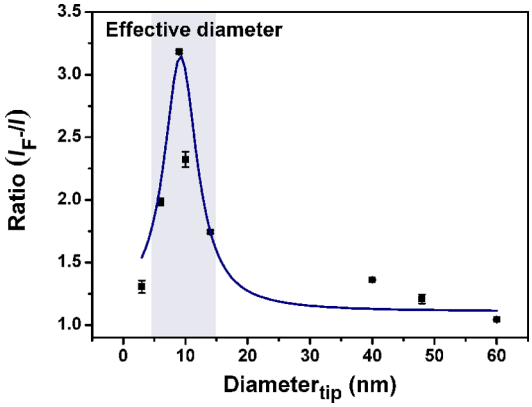

Figure 6. Current ratios ($I_F{}^-/I$) measured at −2.0 V of the APBA-modified nanochannel with different tip diameters.

F^- (0.01 nM, 100 nM, and 1 mM), the mean water contact angle showed a variation trend that first decreased and then increased. When most of the boronic acid was in the form of $RB(OH)_2F^-$, the hydrophilicity of the APBA-modified PI film was optimized; the mean water contact angle was 46 ± 1°. Subsequently, the mean water contact angle of the APBA-modified PI film increased from 46 ± 1° to 56 ± 0.4° upon the conversion of $RB(OH)_2F^-$ to RBF_3^-.

To investigate the impact of nanochannel size on the activation of the fluoride-driven ionic gate, a series of nanochannels with tip diameters ranging from 5 to 60 nm (calculated by eq 1 in the Supporting Information) were obtained for this study. Figure 6 shows the relationship between tip diameter and ionic transport. The current ratios ($I_F{}^-/I$) showed obvious activation with the tip diameter ranging from 6 to 15 nm. The ratio was highest (3.2) when the tip diameter was approximately 9 nm. When the tip diameter of the nanochannel was too small (diameter$_{tip}$ < 6 nm), APBA can easily block the nanochannel, which leads to very low currents after APBA immobilization. Accordingly, F^- cannot easily enter into the nanochannel to react with APBA, resulting in a low current ratio ($I_F{}^-/I$ = 1.3).

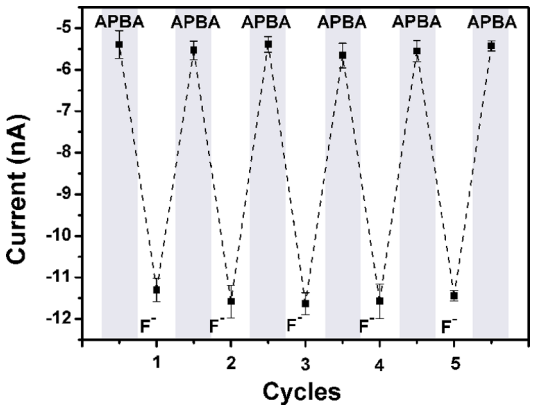

Figure 7. Stability and responsive switchability of the fluoride-driven ionic gate: reversible variation of ionic currents that were measured alternately at −2.0 V with the addition and removal of F^-.

However, charge and wettability variation is nominal for larger diameter nanochannels ($diameter_{tip}$ > 15 nm). Consequently, the current ratios (I_{F^-}/I) drop down to 1.0, indicating that activation can be observed with the tip effective diameter in the range of 6−15 nm.

The smart fluoride-driven ionic gate also has fine stability and cycling performance. The reversibility of the ionic current can be actualized by the addition and removal of F^- (Scheme 1b). As shown in Figure 7, the current of APBA-modified nanochannels dramatically increased to −11.6 nA (down) upon the addition of F^-. The current decreased to −5.4 nA (up) in the absence of F^- after the nanochannel was soaked in alkalescent sodium hydroxide solution (pH 9.5). The *I*−*V* curve was shown in Supporting Information, Figure S5. The hydroxyl replaced fluoride in the way described in the section on current−voltage characteristics at different pH values. At higher pH values, most of the tetrahedral fluoride adduct is converted to $RB(OH)_3^-$. Several cycles later, no damping of the ionic current is observed. Therefore, the APBA-modified nanochannel can be used as a fluoride-driven ionic gate with strong stability and fine responsive switchability.

CONCLUSION

In summary, a fluoride-driven ionic gate was successfully realized by immobilizing 4-aminophenylboronic acid (APBA) onto a single ion track-etched conical nanochannel. This is the first example of an anion regulated synthetic nanochannel. This fluoride-driven ionic gate not only has high sensitivity and particular selectivity to F^-, it also presents excellent responsive switchability and stability. Moreover, this fluoride-driven ionic gate can possibly be used in living systems. Notably, the system is easily visualized through the measuring of ionic currents, free of contamination from aqueous solvents, and environment friendly. Furthermore, the combination of an anion-responsive functional molecule and solid-state synthetic nanochannels enabled the detection of trace elements in a living system. This type of fluoride-driven ionic gate may be used widely, given the importance of fluoride in many fields, including environmental monitoring, clinical medicine, and water quality monitoring.

EXPERIMENTAL SECTION

Materials. Polyimide (PI, Hostaphan RN12 Hoechst, 12-μm thick) film, 1-ethyl-3-(3-dimethyllaminopropyl) carbodiimide (EDC), *N*-hydroxysulfosuccinimide (NHSS), 4-aminophenylboronic acid (APBA), potassium chloride (KCl), sodium hypochlorite (NaClO, 13%), and potassium iodide (KI) were purchased from the Sinopharm Chemical Reagent Beijing Co., Ltd. (SCRC, China). All solutions were prepared with Milli-Q water (18.2 MΩ).

Fabrication. The single conical PI nanochannel was prepared using an asymmetric track-etched technique with a single ion track. Prior to the etching process, each side of the PI film was exposed to UV light (320 nm) for 1 h. The PI film was embedded between the two chambers of a conductivity cell at 60 °C. One chamber was filled with etching solution (NaClO, 13%), while the other chamber was filled with stopping solution (1 M KI). Next, a voltage of 1.0 V was applied across the film. The etching process was stopped at a desired current value corresponding to a certain tip diameter. The diameter of the base was approximately 400 nm, which was measured by scanning electron microscopy (SEM). The diameter of the tip was calculated to be 10 nm (Supporting Information, Figure S1).

Modification. The carboxyl groups were exposed on the nanochannel surface with chemical etching, then APBA was immobilized on the nanochannel surface by a conventional EDC/NHSS cross-linking reaction. The NHSS ester was formed by soaking the PI film in 2 mL of aqueous solution of 30 mg of EDC and 6 mg of NHSS for 1 h. Then, the PI film was washed and treated with 10 mM 4-aminophenylboronic acid solution overnight. Finally, the APBA-modified film was washed three times with distilled water.

Current Measurement. Current−voltage curves were measured with a Keithley 6487 picoammeter (Keithley Instruments, Cleveland, OH). Ionic transport properties were evaluated by the current−voltage (*I*−*V*) curves that were constructed using 0.1 M $NaNO_3$. A single conical nanochannel PI film was mounted between two chambers of the etching cell mentioned above. Ag/AgCl electrodes were used to supply a transmembrane potential across the film. The main transmembrane potential used in this work was a scanning voltage varied from −2.0 to +2.0 V with a 40 s period. The error bars in each figure represent the measuring error of several measurements with the same nanochannel. All measurements were carried out at room temperature.

Optical Properties Measurement. UV−visible absorption spectra were obtained on a PerkinElmer UV−vis spectrometer model Lambda 750. Fluorescence emission spectra were recorded on a FluoroMax-4 spectrofluorometer.

Contact Angles Measurement. Contact angles were measured using an OCA20 instrument (DataPhysics, Germany). The system was maintained at ambient temperature and saturated humidity. In each measurement, a 2 μL droplet of water was dispensed onto the substrates under investigation. The average contact angel value was obtained from five different positions of the same sample. The original PI film for contact angle measurements was treated under the same conditions as the single channel membrane. After that, the sample was treated with deionized water overnight and blown dry with N_2.

XPS and SEM Measurement. X-ray photoelectron spectra (XPS) data were obtained with an ESCALab220i-XL electron spectrometer from VG Scientific set to 300 W Al Kα radiation. All peaks were referenced to C 1s (CHx) at 284.8 eV in the deconvoluted high-resolution C 1s spectra. The analysis software was used as provided by the instrument's manufacturer. SEM measurements were taken in the field-emission mode using a Hitachi S-4800 microscope at an acceleration voltage of 10 kV.

NMR Spectra. ^{1}H and ^{19}F NMR spectra were recorded from samples in D_2O at room temperature on a Bruker DM300 or AV 400 spectrometer. All chemical shifts were quoted in parts per million (ppm).

Conflict of Interest: The authors declare no competing financial interest.

Acknowledgment. This work was supported by the National Research Fund for Fundamental Key Projects (2011CB935703, 2011CB935704), National Natural Science Foundation (21171171, 21434003, 91427303, 21201170, 91127025, 21121001), and the Key Research Program of the Chinese Academy of Sciences (KJZD-EW-M01).

Supporting Information Available: Details of fabrication and characterization, pH-dependent ionic rectification, scanning electron microscopy (SEM) of the conical nanochannel, X-ray photoelectron spectra (XPS) data; channel-to-channel variability and the mean and standard deviations; kinetic response of APBA-modified nanochannel; ^{1}H NMR spectra of APBA with different equiv F^- in D_2O. This material is available free of charge via the Internet at http://pubs.acs.org.

REFERENCES AND NOTES

1. Gadsby, D. C. Ion Transport: Spot the Difference. *Nature* **2004**, *427*, 795–797.
2. He, Z.; Zhou, J.; Lu, X.; Corry, B. Bioinspired Graphene Nanopores with Voltage-Tunable Ion Selectivity for Na^+ and K^+. *ACS Nano* **2013**, *7*, 10148–10157.
3. Mistlberger, G.; Xie, X. J.; Pawlak, M.; Crespo, G. A.; Bakker, E. Photoresponsive Ion Extraction/Release Systems: Dynamic Ion Optodes for Calcium and Sodium Based on Photochromic Spiropyran. *Anal. Chem.* **2013**, *85*, 2983–2990.
4. Tian, Y.; Hou, X.; Wen, L. P.; Guo, W.; Song, Y. L.; Sun, H. Z.; Wang, Y. G.; Jiang, L.; Zhu, D. B. A Biomimetic Zinc Activated Ion Channel. *Chem. Commun.* **2010**, *46*, 1682–1684.
5. Liu, Y.-W.; Chen, C.-H.; Wu, A.-T. A Turn-On and Reversible Fluorescence Sensor for Al^{3+} Ion. *Analyst* **2012**, *137*, 5201–5203.
6. Blas, J. R.; Márquez, M.; Sessler, J. L.; Luque, F. J.; Orozco, M. Theoretical Study of Anion Binding to Calix[4]pyrrole: The Effects of Solvent, Fluorine Substitution, Cosolute, and Water Traces. *J. Am. Chem. Soc.* **2002**, *124*, 12796–12805.
7. Ciardi, M.; Tancini, F.; Gil-Ramírez, G.; Escudero Adán, E. C.; Massera, C.; Dalcanale, E.; Ballester, P. Switching from Separated to Contact Ion-Pair Binding Modes with Diastereomeric Calix[4]pyrrole Bis-phosphonate Receptors. *J. Am. Chem. Soc.* **2012**, *134*, 13121–13132.
8. Gale, P. A.; Sessler, J. L.; Král, V.; Lynch, V. Calix[4]pyrroles: Old Yet New Anion-Binding Agents. *J. Am. Chem. Soc.* **1996**, *118*, 5140–5141.
9. Sessler, J. L.; Gross, D. E.; Cho, W.-S.; Lynch, V. M.; Schmidtchen, F. P.; Bates, G. W.; Light, M. E.; Gale, P. A. Calix[4]pyrrole as a Chloride Anion Receptor: Solvent and Countercation Effects. *J. Am. Chem. Soc.* **2006**, *128*, 12281–12288.
10. Berndt, A.; Lee, S. Y.; Ramakrishnan, C.; Deisseroth, K. Structure-Guided Transformation of Channelrhodopsin into a Light-Activated Chloride Channel. *Science* **2014**, *344*, 420–424.
11. Wietek, J.; Wiegert, J. S.; Adeishvili, N.; Schneider, F.; Watanabe, H.; Tsunoda, S. P.; Vogt, A.; Elstner, M.; Oertner, T. G.; Hegemann, P. Conversion of Channelrhodopsin into a Light-Gated Chloride Channel. *Science* **2014**, *344*, 409–412.
12. Li, Y. P.; Lin, H.; Lin, H. Ratiometric and Selective Fluorescent Sensor for F^- Based on Intramolecular Charge Transfer (ICT). *J. Fluoresc.* **2010**, *20*, 1299–1305.
13. Liang, T.; Neumann, C. N.; Ritter, T. Introduction of Fluorine and Fluorine-Containing Functional Groups. *Angew. Chem., Int. Ed.* **2013**, *52*, 8214–8264.
14. Kleerekoper, M. The Role of Fluoride in the Prevention of Osteoporosis. *Endocrin. Metab. Clin.* **1998**, *27*, 441–452.
15. Mummidivarapu, V. S.; Nehra, A.; Hinge, V. K.; Rao, C. P. Triazole Linked Picolylimine Conjugate of Calix[6]arene as a Sequential Sensor for La^{3+} Followed by F^-. *Org. Lett.* **2012**, *14*, 2968–2971.
16. Yang, X.-F.; Ye, S.-J.; Bai, Q.; Wang, X.-Q. A Fluorescein-Based Fluorogenic Probe for Fluoride Ion Based on the Fluoride-Induced Cleavage of *tert*-Butyldimethylsilyl Ether. *J. Fluoresc.* **2007**, *17*, 81–87.
17. Cooper, C.; James, T. Selective Fluorescence Detection of Fluoride Using Boronic Acids. *Chem. Commun.* **1998**, 1365–1366.
18. Areti, S.; Khedkar, J. K.; Chilukula, R.; Rao, C. P. Thiourea Linked Peracetylated Glucopyranosyl-Anthraquinone Conjugate as Reversible ON-OFF Receptor for Fluoride in Acetonitrile. *Tetrahedron Lett.* **2013**, *54*, 5629–5634.
19. Wickenden, A. D. Potassium Channels as Anti-epileptic Drug Targets. *Neuropharmacology* **2002**, *43*, 1055–1060.
20. Xia, H.; Qin, D. D.; Zhou, X. B.; Liu, X. H.; Lu, X. Q. Ion Transport Traversing Bioinspired Ion Channels at Bionic Interface. *J. Phys. Chem. C* **2013**, *117*, 23522–23528.
21. Dehez, F.; Tarek, M.; Chipot, C. Energetics of Ion Transport in a Peptide Nanotube. *J. Phys. Chem. B* **2007**, *111*, 10633–10635.
22. Hummer, G.; Rasaiah, J. C.; Noworyta, J. P. Water Conduction through the Hydrophobic Channel of a Carbon Nanotube. *Nature* **2001**, *414*, 188–190.
23. Wan, R. Z.; Li, J. Q.; Lu, H. J.; Fang, H. P. Controllable Water Channel Gating of Nanometer Dimensions. *J. Am. Chem. Soc.* **2005**, *127*, 7166–7170.
24. Assouma, C. D.; Crochet, A.; Chérémond, Y.; Giese, B.; Fromm, K. M. Kinetics of Ion Transport through Supramolecular Channels in Single Crystals. *Angew. Chem. Int. Edit* **2013**, *52*, 4682–4685.
25. Bruhova, I.; Zhorov, B. S. KvAP-Based Model of the Pore Region of Shaker Potassium Channel Is Consistent with Cadmium- and Ligand-Binding Experiments. *Biophys. J.* **2005**, *89*, 1020–1029.
26. Wen, L. P.; Jiang, L. Construction of Biomimetic Smart Nanochannels for Confined Water. *Natl. Sci. Rev.* **2014**, *1*, 144–156.
27. Wen, L. P.; Hou, X.; Tian, Y.; Nie, F. Q.; Song, Y. L.; Zhai, J.; Jiang, L. Bioinspired Smart Gating of Nanochannels toward Photoelectric-Conversion Systems. *Adv. Mater.* **2010**, *22*, 1021–1024.
28. Ali, M.; Ramirez, P.; Mafé, S.; Neumann, R.; Ensinger, W. A pH-Tunable Nanofluidic Diode with a Broad Range of Rectifying Properties. *ACS Nano* **2009**, *3*, 603–608.
29. Hou, X.; Liu, Y.; Dong, H.; Yang, F.; Li, L.; Jiang, L. A pH-Gating Ionic Transport Nanodevice: Asymmetric Chemical Modification of Single Nanochannels. *Adv. Mater.* **2010**, *22*, 2440–2443.
30. Yameen, B.; Ali, M.; Neumann, R.; Ensinger, W.; Knoll, W.; Azzaroni, O. Single Conical Nanopores Displaying pH-Tunable Rectifying Characteristics. Manipulating Ionic Transport with Zwitterionic Polymer Brushes. *J. Am. Chem. Soc.* **2009**, *131*, 2070–2071.
31. Zeng, Z. P.; Ai, Y.; Qian, S. Z. pH-Regulated Ionic Current Rectification in Conical Nanopores Functionalized with Polyelectrolyte Brushes. *Phys. Chem. Chem. Phys.* **2014**, *16*, 2465–2474.
32. Hou, X.; Yang, F.; Li, L.; Song, Y. L.; Jiang, L.; Zhu, D. B. A Biomimetic Asymmetric Responsive Single Nanochannel. *J. Am. Chem. Soc.* **2010**, *132*, 11736–11742.
33. Yameen, B.; Ali, M.; Neumann, R.; Ensinger, W.; Knoll, W.; Azzaroni, O. Ionic Transport through Single Solid-State Nanopores Controlled with Thermally Nanoactuated Macromolecular Gates. *Small* **2009**, *5*, 1287–1291.

34. Abelow, A. E.; Schepelina, O.; White, R. J.; Vallée-Bélisle, A.; Plaxco, K. W.; Zharov, I. Biomimetic Glass Nanopores Employing Aptamer Gates Responsive to a Small Molecule. *Chem. Commun.* **2010**, *46*, 7984–7986.
35. Han, C. P.; Hou, X.; Zhang, H. C.; Guo, W.; Li, H. B.; Jiang, L. Enantioselective Recognition in Biomimetic Single Artificial Nanochannels. *J. Am. Chem. Soc.* **2011**, *133*, 7644–7647.
36. Heins, E. A.; Baker, L. A.; Siwy, Z. S.; Mota, M. O.; Martin, C. R. Effect of Crown Ether on Ion Currents through Synthetic Membranes Containing a Single Conically Shaped Nanopore. *J. Phys. Chem. B* **2005**, *109*, 18400–18407.
37. Vlassiouk, I.; Park, C.-D.; Vail, S. A.; Gust, D.; Smirnov, S. Control of Nanopore Wetting by a Photochromic Spiropyran: A Light-Controlled Valve and Electrical Switch. *Nano Lett.* **2006**, *6*, 1013–1017.
38. Wen, L. P.; Liu, Q.; Ma, J.; Tian, Y.; Li, C. H.; Bo, Z. S.; Jiang, L. Malachite Green Derivative-Functionalized Single Nanochannel: Light-and-pH Dual-Driven Ionic Gating. *Adv. Mater.* **2012**, *24*, 6193–6198.
39. Wen, L. P.; Ma, J.; Tian, Y.; Zhai, J.; Jiang, L. A Photo-Induced, and Chemical-Driven, Smart-Gating Nanochannel. *Small* **2012**, *8*, 838–842.
40. Kalman, E. B.; Sudre, O.; Vlassiouk, I.; Siwy, Z. S. Control of Ionic Transport through Gated Single Conical Nanopores. *Anal. Bioanal. Chem.* **2009**, *394*, 413–419.
41. Buchsbaum, S. F.; Nguyen, G.; Howorka, S.; Siwy, Z. S. DNA-Modified Polymer Pores Allow pH- and Voltage-Gated Control of Channel Flux. *J. Am. Chem. Soc.* **2014**, *136*, 9902–9905.
42. He, Y.; Gillespie, D.; Boda, D.; Vlassiouk, I.; Eisenberg, R. S.; Siwy, Z. S. Tuning Transport Properties of Nanofluidic Devices with Local Charge Inversion. *J. Am. Chem. Soc.* **2009**, *131*, 5194–5202.
43. Powell, M. R.; Sullivan, M.; Vlassiouk, I.; Constantin, D.; Sudre, O.; Martens, C. C.; Eisenberg, R. S.; Siwy, Z. S. Nanoprecipitation-Assisted Ion Current Oscillations. *Nat. Nanotechnol.* **2008**, *3*, 51–57.
44. Ali, M.; Yameen, B.; Cervera, J.; Ramirez, P.; Neumann, R.; Ensinger, W.; Knoll, W.; Azzaroni, O. Layer-by-Layer Assembly of Polyelectrolytes into Ionic Current Rectifying Solid-State Nanopores: Insights from Theory and Experiment. *J. Am. Chem. Soc.* **2010**, *132*, 8338–8348.
45. Smirnov, S. N.; Vlassiouk, I. V.; Lavrik, N. V. Voltage-Gated Hydrophobic Nanopores. *ACS Nano* **2011**, *5*, 7453–7461.
46. Striemer, C. C.; Gaborski, T. R.; McGrath, J. L.; Fauchet, P. M. Charge- and Size-Based Separation of Macromolecules Using Ultrathin Silicon Membranes. *Nature* **2007**, *445*, 749–753.
47. Zhou, K.; Kovarik, M. L.; Jacobson, S. C. Surface-Charge Induced Ion Depletion and Sample Stacking Near Single Nanopores in Microfluidic Devices. *J. Am. Chem. Soc.* **2008**, *130*, 8614–8616.
48. Luo, L.; Holden, D. A.; White, H. S. Negative Differential Electrolyte Resistance in a Solid-State Nanopore Resulting from Electroosmotic Flow Bistability. *ACS Nano* **2014**, *8*, 3023–3030.
49. Hou, X.; Guo, W.; Xia, F.; Nie, F. Q.; Dong, H.; Tian, Y.; Wen, L. P.; Wang, L.; Cao, L. X.; Yang, Y. A Biomimetic Potassium Responsive Nanochannel: G-Quadruplex DNA Conformational Switching in a Synthetic Nanopore. *J. Am. Chem. Soc.* **2009**, *131*, 7800–7805.
50. Tian, Y.; Zhang, Z.; Wen, L. P.; Ma, J.; Zhang, Y. Q.; Liu, W. D.; Zhai, J.; Jiang, L. A Biomimetic Mercury (II)-Gated Single Nanochannel. *Chem. Commun.* **2013**, *49*, 10679–10681.
51. Ali, M.; Nasir, S.; Ramirez, P.; Cervera, J.; Mafe, S.; Ensinger, W. Calcium Binding and Ionic Conduction in Single Conical Nanopores with Polyacid Chains: Model and Experiments. *ACS Nano* **2012**, *6*, 9247–9257.
52. Zhao, C.; Li, X. S.; Li, L. Y.; Gong, X.; Chang, Y.; Zheng, J. Mimicking the Binding and Unbinding of Fe^{3+} with Transferrin Using a Single Biomimetic Nanochannel. *Chem. Commun.* **2013**, *49*, 9317–9319.
53. Bondy, C. R.; Loeb, S. J. Amide Based Receptors for Anions. *Coord. Chem. Rev.* **2003**, *240*, 77–99.
54. Chmielewski, M. J.; Jurczak, J. Anion Recognition by Neutral Macrocyclic Amides. *Chem—Eur. J.* **2005**, *11*, 6080–6094.
55. Kang, S. O.; Llinares, J. M.; Powell, D.; VanderVelde, D.; Bowman-James, K. New Polyamide Cryptand for Anion Binding. *J. Am. Chem. Soc.* **2003**, *125*, 10152–10153.
56. Dusemund, C.; Sandanayake, K. S.; Shinkai, S. Selective Fluoride Recognition with Ferroceneboronic Acid. *J. Chem. Soc., Chem. Commun.* **1995**, 333–334.
57. Galbraith, E.; James, T. D. Boron Based Anion Receptors as Sensors. *Chem. Soc. Rev.* **2010**, *39*, 3831–3842.
58. Koskela, S. J.; Fyles, T. M.; James, T. D. A Ditopic Fluorescent Sensor for Potassium Fluoride. *Chem. Commun.* **2005**, 945–947.
59. Sharma, D.; Sahoo, S. K.; Chaudhary, S.; Bera, K. R.; Callan, J. F. Fluorescence 'Turn-On' Sensor for F^- Derived from Vitamin B6 Cofactor. *Analyst* **2013**, *138*, 3646–3650.
60. Sessler, J. L.; Camiolo, S.; Gale, P. A. Pyrrolic and Polypyrrolic Anion Binding Agents. *Coord. Chem. Rev.* **2003**, *240*, 17–55.
61. Wongsan, W.; Aeungmaitrepirom, W.; Chailapakul, O.; Ngeontae, W.; Tuntulani, T. Bifunctional Polymeric Membrane Ion Selective Electrodes Using Phenylboronic Acid as a Precursor of Anionic Sites and Fluoride as an Effector: A Potentiometric Sensor for Sodium Ion and an Impedimetric Sensor for Fluoride Ion. *Electrochim. Acta* **2013**, *111*, 234–241.
62. Siwy, Z. S. Ion-Current Rectification in Nanopores and Nanotubes with Broken Symmetry. *Adv. Funct. Mater.* **2006**, *16*, 735–746.
63. Xu, Z. C.; Kim, S. K.; Han, S. J.; Lee, C.; Kociok-Kohn, G.; James, T. D.; Yoon, J. Ratiometric Fluorescence Sensing of Fluoride Ions by an Asymmetric Bidentate Receptor Containing a Boronic Acid and Imidazolium Group. *Eur. J. Org. Chem.* **2009**, *2009*, 3058–3065.
64. Butters, M.; Harvey, J. N.; Jover, J.; Lennox, A. J. J.; Lloyd-Jones, G. C.; Murray, P. M. Aryl Trifluoroborates in Suzuki−Miyaura Coupling: The Roles of Endogenous Aryl Boronic Acid and Fluoride. *Angew. Chem., Int. Ed.* **2010**, *49*, 5156–5160.
65. Molander, G. A.; Cavalcanti, L. N.; García-García, C. Nickel-Catalyzed Borylation of Halides and Pseudohalides with Tetrahydroxydiboron $[B_2(OH)_4]$. *J. Org. Chem.* **2013**, *78*, 6427–6439.
66. Molander, G. A.; Trice, S. L. J.; Kennedy, S. M. Palladium-Catalyzed Borylation of Aryl and Heteroaryl Halides Utilizing Tetrakis(dimethylamino)diboron: One Step Greener. *Org. Lett.* **2012**, *14*, 4814–4817.
67. Yamaguchi, S.; Akiyama, S.; Tamao, K. Colorimetric Fluoride Ion Sensing by Boron-Containing π-Electron Systems. *J. Am. Chem. Soc.* **2001**, *123*, 11372–11375.
68. Liu, Z.-Q.; Shi, M.; Li, F.-Y.; Fang, Q.; Chen, Z.-H.; Yi, T.; Huang, C.-H. Highly Selective Two-Photon Chemosensors for Fluoride Derived from Organic Boranes. *Org. Lett.* **2005**, *7*, 5481–5484.